Insight into electroreductive activation process of peroxydisulfate for eliminating organic pollution: Essential role of atomic hydrogen

Zeng Huabin, Lan Huachun, An Xiaoqiang, Repo Eveliina, Park Yuri, Pastushok Olga, Liu Huijuan, Qu Jiuhui

DOI: 10.1016/j.cej.2020.128355

Insight into Electroreductive Activation Process of Peroxydisulfate for Eliminating Organic Pollution: Essential Role of Atomic Hydrogen

Huabin Zeng,[a,b] Huachun Lan,[a*] Xiaoqiang An,[a] Eveliina Repo,[b] Yuri Park,[b] Olga Pastushok,[b] Huijuan Liu,[a] Jiuhui Qu[a]

[a] Center for Water and Ecology, State Key Joint Laboratory of Environment Simulation and Pollution Control, School of Environment, Tsinghua University, Beijing 100084, China

[b] Department of Separation Science, School of Engineering Science, Lappeenranta-Lahti University of Technology LUT, Sammonkatu 12, FI-50130 Mikkeli, Finland

*Corresponding author:

Center for Water and Ecology, State Key Joint Laboratory of Environment Simulation and Pollution Control,

School of Environment, Tsinghua University,

Beijing 100084, China

E-mail address: hclan@tsinghua.edu.cn

Table of Contents/Abstract Art

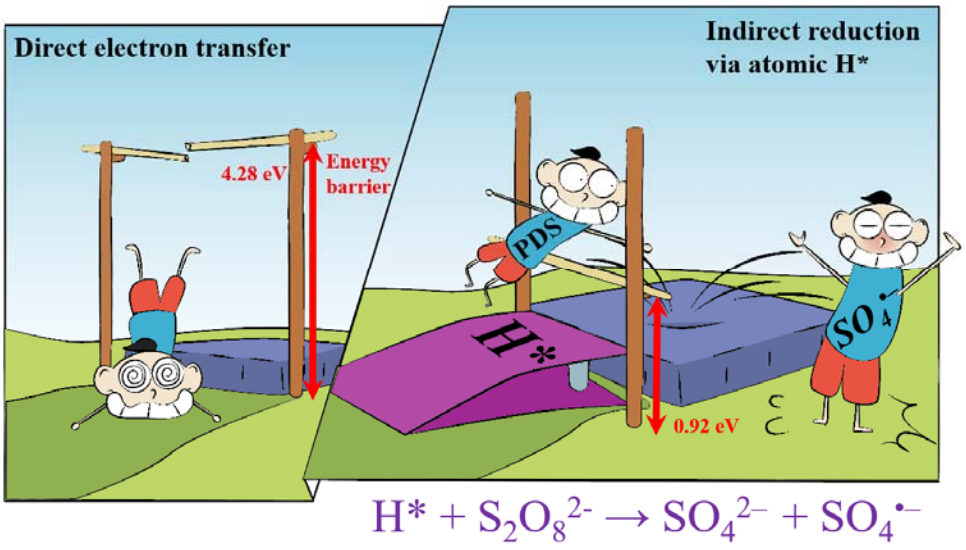

Abstract

Electrochemically activating peroxydisulfate (PDS) can eliminate organic pollution using electron as activator without the involvement of byproducts. Notwithstanding, the process suffered from long hydraulic retention time, and the activation regime remained unclear. Herein, using Pd/Al_2O_3 catalyst as particle electrode for initiating PDS oxidation in the cathodic cell can degrade various organic pollutants with varying the kinetic constants from 0.0256 min^{-1} to 0.0645 min^{-1}, which were at least 5-fold higher than that in previous studies. The reactive oxygen species were determined to be $SO_4^{\bullet-}$/$^{\bullet}OH$. These radicals were readily formed from the single-electron reduction of PDS by electro-induced atomic hydrogen (indirect reduction mechanism), while direct two-electron transfer from electro-generated H_2 to PDS consumed its oxidation capacity without yielding radical due to the higher energy barrier. Revealing the mechanism of electrochemically unleashing the oxidative power of PDS into $SO_4^{\bullet-}$ can rationalize the design of scalable electrode for PDS-based water purification.

Keywords: Organic pollution, peroxydisulfate, electroreductive activation, single electron transfer, atomic hydrogen

1. Introduction

By producing strongly oxidizing radicals, advanced oxidation processes (AOPs) were appealing treatment processes for degrading non-biodegradable, recalcitrant and toxic organic contaminants [1]. Recently, peroxydisulfate (PDS, $S_2O_8^{2-}$) attracted growing attention as a promising oxidant not only due to its chemical stability in the storage and transport periods but also owing to highly achievable radical formation yield [2]. Moreover, the produced sulfate radical ($SO_4^{\bullet-}$) demonstrated longer lifetime than hydroxyl radicals ($^{\bullet}OH$) in water (30 μs for $SO_4^{\bullet-}$ and 1 μs for $^{\bullet}OH$) [3], as well as less dependence of treatment efficiency on the operational parameters (e.g. pH, initial peroxide loading, and background constituents) [2]. These properties endowed the PDS with bright application perspective in the soil remediation and water treatment.

$$S_2O_8^{2-} + \text{energy} \rightarrow 2\ SO_4^{\bullet-} \quad (1)$$

$$S_2O_8^{2-} + M^{n+} \rightarrow M^{(n+1)+} + SO_4^{2-} + SO_4^{\bullet-} \quad (2)$$

$$S_2O_8^{2-} + e^- \rightarrow SO_4^{2-} + SO_4^{\bullet-} \quad (3)$$

For extending the application scenarios of PDS oxidation, the suitable activation approach for environmental problem has been a “holy grail” in these scientific researches [2]. Generally, the $S_2O_8^{2-}$ activation to $SO_4^{\bullet-}$ can be initiated by energy input (heat, microwave, or light) or single-electron transfer from transition metal catalysts (M=Fe, Co, Cu, Ag) (**reaction 1~2**) [4]. Among these approaches, the PDS activation by transition metal catalysts has been widely employed for application of PDS in *in-situ* chemical oxidation of polluted areas [5, 6]. In addition, the electrochemical activation of PDS via one-electron reduction on the cathode (**reaction 3**) attracted some attention [7-9], owing to the reagent-free property using electron as reductant without the involvement of byproducts, preventing the costly transportation and storage on the activators and the downstream treatment for removing the byproducts, as well as reducing the dependence on the

operating pH [9]. Meanwhile, remotely electrolytic manipulation toward the PDS activation theoretically allowed the environmental remediation process to be precisely controlled by tuning the applied potential [10, 11]. Despite these advantages, the degradation kinetics of most organic compounds (dinitrotoluene, aniline, and ciprofloxacin,) were much slower than those for PDS oxidation initiated by transition metal activators, and the process exhibited meaningful degradation only within an irrational time scale (more than 6 hours) [7-9]. More importantly, these works were confined to revealing the phenomena of heterolytically cleaving the peroxide bond for yielding $SO_4^{\bullet-}$ by single-electron injection from carbon cathode into PDS molecule (**reaction 3**). The studies never unravel the active sites for PDS reaction and key intermedia for single-electron transfer except in cases where pH-sensitive Fe^{2+}/Fe^{3+} bridged between electrode and PDS [12]. The insight into the electrochemical activation mechanism without iron will facilitate the rational design of an electro-AOP for efficiently utilizing PDS.

It has been well-documented that the electrocatalytic reduction of substrates can proceed through both direct electron transfer and indirect mechanism via atomic hydrogen (atomic H*) [13]. Depending on using the electrode surface or the electro-generated atomic H* as a platform for adsorption of substrates, the subsequent conversion may be steered towards the different routes with yielding different products. In our case, we were particularly intrigued by atomic H* due to its unique nature as a one-electron reductant. Especially, much lower redox potential of H^*/H^+ couple (E° = -2.1 V vs RHE) than that of Fe^{2+}/Fe^{3+} couple (E° = -0.77 V vs RHE) indicated that PDS reduction by atomic H* was thermodynamically feasible with $SO_4^{\bullet-}$ as reduction product (**Reaction 4**) [14, 15]. Among various materials for atomic H* generation, the most presentative ones were palladium (Pd) and its alloys, for their outstanding electronic property to form relatively stable Pd-H* bond (Volmer reaction) [16], and depress the recombination of two atomic H*

(Heyrovsky reaction), therefore to extend the retention time of atomic H* [17-19]. The lab-scale experiments using Pd-doping cathode (two-dimensional electrode, 2D electrode) or Pd-coating particle electrode (three-dimensional electrode, 3D electrode) have been deemed atomic-H*-rich systems for dechlorination of disinfection by-products and dehydrogenation of various unsaturated organics [20]. In comparison to 2D electrochemical system, the electroreduction system with 3D electrode theoretically provided more active sites for generating atomic H*, which may lead to higher kinetic constant of substrate reduction in the system.

$$S_2O_8^{2-} + H^* \rightarrow H^+ + SO_4^{2-} + SO_4^{\bullet-} \quad (4)$$

In this work, a 3D electroreduction system using commercial Pd/Al_2O_3 as particle electrode was applied for investigating the mechanism of PDS reduction. Meanwhile, externally added BA (50 μM) was employed as a probe for efficiently capturing $SO_4^{\bullet-}$ in the PDS decomposition process (k=1.2×10^9 $M^{-1}\cdot s^{-1}$) [12, 21], while it showed inertness to atomic H* produced on the Pd/Al_2O_3 [12]. The PDS decompositions via single-electron/two-electron reduction routes were clarified by electron spin resonance (ESR) analysis, quenching experiments, and density function theory (DFT) calculations. The involved parameters were optimized for accelerating PDS activation. Finally, the practical value of the system was further assessed by degrading various organic contaminants.

2. Experimental Section

2.1 Chemicals

A complete list of reagents is provided in **Text S1 (Supplementary Material)**.

2.2 Setup of batch Experiment

Solutions in this study were prepared using deionized (DI) water (resistivity 18.2 MΩ, arium® pro system). Solution pH regulation was performed using NaOH or H_2SO_4.

Experiments were conducted in a two-cell electrochemical reactor, a schematic diagram of which

is presented in **Figure S1**. Before the reactor was used, N_2 was used to flush out the air in the cathodic cell. The liquid samples were preserved in the 1 M ethanol solution once the sample was taken from the reactor.

2.3 Analytical Method

The concentrations of model contaminants were measured by high-performance liquid chromatography (HPLC, Shimadzu LC-20AD, Tokyo, Japan) with a C18 column and ultraviolet detector, the temperature of column was kept at 30 ℃ and the mobile phase was maintained at a flow rate of 1.0 ml/min. Other analytical details about HPLC analysis of organic contaminants were presented in the **Table S1,** including mobile phase and detecting wavelengths.

The PDS concentration was determined colorimetrically using potassium titanium oxalate solution at a wavelength of 352 nm by ultraviolet spectrophotometer (lambda 45, PerkinElmer) and the detection method was described in detail by Zeng et al [22].

The formation of reactive oxygen species (ROS) was identified with an ESR spectrometer (CMS 8400, Adani). For $OH\cdot$ and $SO_4^{\cdot-}$ measurements, the sample was immediately mixed with DMPO to form adducts. The phase composition of the synthesised catalyst was studied by X-ray diffractometer (XRD, PANalytical), using Co-Kα radiation (λ=0.1789 nm, at 40 kV and 40 mA) over a 2θ range of 10~120° with a step size of 0.02° and scan speed of 2°/min.

2.4 DFT analysis

The surface of Pd (111) was built, where the vacuum space along the z-direction is set to be 20 Å, eliminating the interaction between two neighboring images. The bottom two atomic layers were fixed, the top three atomic layers were adequately relaxed for all surface systems. Then the atom, ion and molecular were adsorbed on the surface. The first-principles calculations in the framework of DFT were carried out based on the Cambridge Sequential Total Energy Package (CASTEP)

[23]. The exchange-correlation functional under the generalized gradient approximation (GGA) with norm-conserving pseudopotentials [24], and Perdew-Burke-Ernzerhof functional was adopted to describe the electron-electron interaction [25]. An energy cutoff of 750 eV was used and a k-point sampling set of 5×5×1 were tested to be converged. A force tolerance of 0.01 eV/Å, energy tolerance of 5.0×10^{-7} eV per atom and maximum displacement of 5.0×10^{-4} Å were considered. The transition states are calculated with the complete LST/QST search.

The adsorption energy of were calculated by: $\Delta E_A = E^*_A - E^* - E_A$

where E^*_A, E^* and E_A denote the energy of adsorbed system, clear surface and absorbed atom, ion or molecular, respectively [26].

3. Results and discussion

3.1 PDS Activation by Pd/Al_2O_3 in Electroreduction System.

The physicochemical properties of the Pd/Al_2O_3 catalyst and its corresponding substrate (α-Al_2O_3) were characterized by SEM, XPS, and XRD analysis. SEM results (**Fig. 1b**) presented that many flower-like particles were attached to the relatively smooth surface of the particle presented in **Fig. 1a** (SEM analysis of α-Al_2O_3 substrate). These particles can be determined to be dominant Pd^0 speciation (335.2 eV for Pd^0 $3d_{5/3}$ and 340.5 eV for Pd^0 $3d_{2/3}$) by XPS analysis (**Fig. 1c**) [27]. Meanwhile, the coverage of the Pd crystal on the surface slightly impaired the acquisition of Al_2O_3-involving signals (74.7 eV for Al^{3+} 2p and 351.6 eV for O^{2-} 1s, **Fig. 1c inset**) [28]. Furthermore, comparing the XRD results of Pd/Al_2O_3 catalyst with α-Al_2O_3 substrate revealed the face-centered cubic structure of coated Pd catalyst (**Fig. 1d**). The emerging peak of Pd/Al_2O_3 at 39.4˚ can be assigned to the Pd(111) of metallic Pd crystal.

Theoretically, the dominant exposure of the Pd(111) facet can provide ideal active sites for producing atomic H* [29]. The atomic H* provision capacity of Pd/Al_2O_3 catalyst was further evaluated by the cyclic voltammetry (CV) curves using Pd/Al_2O_3-coating glassy carbon electrode as working electrode (**Text S2**). With varying starting potentials from -0.65 V to -0.80 V during CV analysis, the generated H* species in the reduction stage were oxidized in oxidation stage. **Fig. 1e** exhibited two oxidation peaks in positive scans, located in the potential ranges of −0.30 to −0.10 V and −0.10 to 0.10 V. By the addition of atomic H* scavenger (2,4-dichlorophenol, 2,4-DCP) [18], the peak at -0.10 V can be assigned to adsorbed H^*_{ads} while the peak at -0.30 V referred to the oxidation of absorbed H^*_{abs}. As shown in **Fig. 1f**, the height of the oxidation peaks for these atomic H* (H^*_{abs} and H^*_{ads}) significantly increased with a decreasing starting potential. The results suggested that the Pd/Al_2O_3 catalyst had plenty of active sites for H*, indicative of good testing platform for PDS activation by atomic H*.

Then, we conducted an experiment in the cathodic compartment to investigate feasibility of BA degradation ($C_{initial}$=50 μM) and simultaneous decomposition of PDS ($C_{initial}$=20 mM) in the Pd/Al_2O_3-enhanced electroreduction system (Pd/ER/PDS system), *i. e.* in addition to a constant current applied on the cathode (100 mA), the reaction suspension contained Pd/Al_2O_3 as particle electrode (0.5 g/L catalyst, pH of 3.0, and deoxygenated atmosphere). As shown in **Fig. 2**, 45.08% of BA in the Pd/ER system was rapidly degraded at a first-order kinetic constant of 0.0097 min^{-1} (k_1, R^2=0.9965). For demonstrating the role of these elements, Pd/PDS system and ER/Pd system showed no performance on the BA degradation, ruling out the feasibility of PDS activation by Pd/Al_2O_3 and BA degradation by atomic H*. Aforementioned results revealed that a synergetic activation of PDS occurs between Pd catalyst and ER system within the time scale. Meanwhile, we monitored the variation of PDS concentration as a function of time. As we supposed above that

PDS may serve as an oxidant for organic degradation, simultaneous PDS decomposition was observed with a zero-order kinetic constant of 0.3002 $mM \cdot min^{-1}$ (k_0, R^2=0.9971).

3.2 ROS analysis

ESR analysis was employed directly identifying ROS for BA oxidation using DMPO as a spin-trapping reagent. As displayed in **Fig. 3a**, nine characteristic peaks of DMPO−H were observed in the Pd/ER system, indicative of atomic H* formation [13]. With the addition of PDS, both DMPO−SO_4 and DMPO−OH adducts were clearly detected whereas signals of DMPO−H disappeared, proving the occurrence of $SO_4^{\bullet-}$ and its symbiotic radical ($^{\bullet}OH$) in our system (**reaction 5**) [22]. It has been well-documented that atomic H* can be generated in the 3D electrochemical system that contained Pd-involved particle electrode [20, 30]. Similar to Fe^{2+} (most presentative single-electron medium for activation of peroxide compounds), atomic H* as a single-electron reductant can asymmetrically cleavage the peroxide bond in the $S_2O_8^{2-}$ ions and forms $SO_4^{\bullet-}$ for oxidizing BA (**reaction 6**). The quenching experiment using ethanol as a scavenger for both $SO_4^{\bullet-}$ and $^{\bullet}OH$ further confirmed the dominant role of these radicals played in the BA degradation process (**Fig. 3b, Fig. S3a**) [12]. Comparing the inhibitory effects of ethanol and TBA on the BA degradation unraveled the importance of atomic H* on the PDS activation (**Fig. 3b, Fig. S4a**). As a quenching agent for $^{\bullet}OH$ and atomic H*, TBA showed much lower reactivity with $SO_4^{\bullet-}$ (**Table S2**) [31]. Therefore, this should have suggested a slighter inhibition of organic abatement by TBA than that by ethanol in the $SO_4^{\bullet-}$-based oxidation process, as evidenced by other researchers [32]. However, our experiment batch for BA degradation with TBA addition demonstrated a lower k_1-value than that with the addition of ethanol in this system, which may arise from the simultaneous quenching on both oxidizing radical generation from atomic H* and BA oxidation by $^{\bullet}OH$. The abnormal results reflected the necessity of atomic H* for the PDS

activation.

$$SO_4^{\bullet-} + OH^- \rightarrow SO_4^{2-} + {}^{\bullet}OH \quad (5)$$

$$\equiv Pd\text{-}H^* + S_2O_8^{2-} \rightarrow \equiv Pd + H^+ + SO_4^{2-} + SO_4^{\bullet-} \quad (6)$$

$$\equiv Pd\text{-}H^* + SO_4^{\bullet-} \rightarrow \equiv Pd + H^+ + SO_4^{2-} \quad (7)$$

Based on the data in **Fig. 2**, the ratio of Δc(PDS)/Δc(BA) was estimated to be around 700, which was close to the values in the literatures [7-9], indicating a low utilization efficiency of PDS for oxidizing organics. The low utilization efficiency might be due that excess atomic H* may quench the generated $SO_4^{\bullet-}$ (**reaction 7**) and inhibit organics' decontamination (similar to excess Fe^{2+} in Fenton process) [33], or that oxidation capacity of PDS could be consumed by directly abstracting two-electrons via a non-radical approach. The monitoring on PDS decay supplied some evidences for this. As displayed in **Fig. 3b**, although TBA efficiently inhibited atomic H*, the TBA addition of various concentrations showed almost no influence on the PDS degradation. The result ruled out the mechanism for PDS consumption via a two-step reduction of two atomic H* and implied another PDS decomposition approach.

3.3 DFT analysis

For better elucidating the PDS decomposition on the Pd/Al_2O_3, DFT analysis was conducted to connect the decomposition approaches of PDS with two electroreduction routes. In the analysis, a hyphen stood for the states where two units bonded with each other, whereas the plug sign presented the separate state. A Pd(111) facet was constructed as the representative role of Pd/Al_2O_3 catalyst, since the facet was revealed as the most exposed crystal faces by XRD analysis. In the proposed indirect reduction mechanism via atomic H*, the H^+ ions were firstly adsorbed on the Pd atom with a Free Gibbs energy change (ΔG) of -1.324 eV, the negative value indicated that the physical adsorption step can proceed spontaneously (**Fig. 4**). Later, the adsorbed H^+ ion accepted

one electron from Pd catalyst, then was converted into atomic H* through the formation of Pd-H* bond (ΔG=0.232 eV). Subsequently, the $S_2O_8^{2-}$ ion in the bulk solution coupled with atomic H* on the Pd surface to form ≡Pd-H*-$S_2O_8^{2-}$ adduct (ΔG=-3.321 eV), followed by the formation of a transition state structure (TS1) (ΔG=0.916 eV). The drastic decrease of the Gibbs free energy for forming ≡Pd-H*-$S_2O_8^{2-}$ implied the strong bond between atomic H* and $S_2O_8^{2-}$. As shown in **Fig. S5**, charge density difference analysis revealed that the electron density around $S_2O_8^{2-}$ molecule went up with the formation of ≡Pd-H*-$S_2O_8^{2-}$ adduct while the electron density around Pd-H* went down, suggesting an obvious injection of electron into PDS from ≡Pd-H*. Meanwhile, the bond length of the peroxide bridge in the $S_2O_8^{2-}$ ions is stretched from 1.347Å to 1.498Å upon $S_2O_8^{2-}$ adsorption on the atomic H*, indicating the subsequent cleavage of peroxide bond and formation of the ≡Pd-HSO_4^- and desired $SO_4^{\bullet-}$. The step where TS1 was formed was confirmed as the determining step through the reaction channel, due to its highest positive ΔG among these elementary reactions (ΔG_{ds}) [19]. Only when the system overcame the uphill energy barrier, the reaction proceeded fluently. More specifically, the determining step became the "neck of the funnel" for kinetics of PDS activation by atomic H*, determining the kinetic constant for the whole process according to the Arrhenius equation [34].

We then investigated the PDS reduction via direct electron transfer and supposed $SO_4^{\bullet-}$ as the product. In this case, the Pd atoms can be directly employed as the active sites for the PDS adsorption (ΔG = –5.977 eV). With the optimization of the molecule model, the peroxide bond was cleaved and then converted into two less oxidative ≡Pd-$SO_4^{\bullet-}$ [35]. By single-electron transfer, PDS decomposition can be oriented towards $SO_4^{\bullet-}$, presenting highly oxidative capacity when the $SO_4^{\bullet-}$ de-adsorbed from the Pd catalyst. However, the ΔG_{ds} for this reaction channel (4.281 eV) was much higher than ΔG_{ds} for PDS activation by atomic H*, denying the direct electron transfer

mechanism for $SO_4^{\bullet-}$ production and confirming that the atomic H* can orient the PDS reduction towards desired $SO_4^{\bullet-}$. In contrast, if the product was supposed to be SO_4^{2-}, the ΔGds for the channel was just 0.539 eV, suggesting the reasonable reaction route for direct two-electron transfer mechanism.

PDS activation can be efficiently initiated by single-electron transfer, whereas it lost the total oxidation capacity via a two-electron abstraction approach. It can be concluded from the DFT results that the electrochemical system met the necessity for single-electron transfer using atomic H^* as "stepping stone" (indirect reduction mechanism), by contrast, the reduction via direct electron transfer approach tended to consecutively donate two electrons to the adsorbed PDS on the Pd catalyst.

3.4 Electron donor analysis

We optimized the parameters for PDS degradation and $SO_4^{\bullet-}$ production in the Pd/ER system. Original data were displayed in **Fig. S6~S8**, and involved kinetics constants were summarized in **Table 1**. The PDS decay exhibited proportional degradation rates to applied current, which directly refers to the H_2 yield in the system (**Batch No. 1~3**). The positive correlation can be explained by that the H_2 played the role as a two-electron donor in the process through direct electron transfer mechanism. By contrast, the k_0-value for PDS decay was revealed to be kept at a certain value (about 0.3000 $M \cdot min^{-1}$), even with varying PDS and Pd/Al_2O_3 dosage (**Batch No. 1, 4~8**). The independence of PDS decay on these two parameters indicates that the PDS reaction with H_2 occurs at an extremely high speed. Moreover, comparing these influence factors revealed that the PDS diffusion was not the rate-limiting step under these conditions. Interestingly, the BA degradation exhibited different trends towards these influence factors, which characterizes the $SO_4^{\bullet-}$ production in the process. Higher applied current (or applied potential) and higher Pd/Al_2O_3

dosage endowed the BA degradation process higher kinetic constant (k_1), while the k_1 remained unaffected by varying PDS concentration.

It was frequently mentioned in the literatures that atomic H* can be generated from the adsorptive dissociation of electro-generated H_2 (**reaction 8**) or H^+ reduction by capturing the Pd-trapping electron (electro-induced atomic H^*, **reaction 9**) in the 3D ER system [12, 30, 36, 37]. For clarifying the interaction of PDS with active hydrogen species, we purged H_2 into reaction liquid containing BA as $SO_4^{\bullet-}$ probe, PDS as oxidant, and Pd/Al_2O_3 as catalyst. By this way, we excluded the electro-induced atomic H* and deepened the insight into the H_2-initiated PDS degradation process (**Fig. 5**). Interestingly, the PDS was rapidly decomposed without variation of BA concentration, indicative of a non-radical process between PDS and active H_2. Unlike conventionally believed idea that H_2 reduced pollutants via dissociative formation of atomic H*, adsorbed H_2 molecule with assistance of Pd catalyst can directly act as a two-electron donor (H_2^*, **reaction 10**) without necessity to form atomic H* [18]. Additionally, we designed a three-cell electrochemical reactor where only electro-induced atomic H* occurred in the middle cell. In this case, the BA degradation at sacrifice of trace PDS suggested successful production of $SO_4^{\bullet-}$ via efficient activation of PDS by electro-induced atomic H*.

$$\equiv Pd + H_2 \rightarrow 2 \equiv Pd\text{-}H^* \quad (8)$$

$$\equiv Pd + e^- + H^+ \rightarrow \equiv Pd\text{-}H^* \quad (9)$$

$$\equiv Pd + H_2 \rightarrow \equiv Pd\text{-}H_2^* \quad (10)$$

Aforementioned statement clearly unraveled two electron donors for PDS attenuation in the 3D electroreduction system, one was H_2 that inactivated the PDS via direct two-electron transfer, the other was electro-induced atomic H* that allowed valid activation of PDS via single-electron transfer. The H_2 yield was decided by the applied current, while the atomic H* by electro-induction

theoretically depended on the electric field and concentration of particle electrode. Unfortunately, the electrical double layer near the electrode mostly attenuated the electricpotential, while only finite electricpotential difference was used for constructing the electric field, which was the driving force source for ions directional migration to form current. It was impossible to minimize the H_2 yield and increase the proportion of atomic H* by simply adjust the applied potential/current, further improving the PDS activation efficiency. By contrast, increasing the Pd/Al_2O_3 dosage to 1.0 g/L can readily induce higher $SO_4^{\bullet-}$ level by providing more active sites for yielding more atomic H*, simultaneously increasing the organic degradation kinetics and PDS utilization efficiency.

3.5 Application analysis

The research unraveled the mechanism for PDS activation in an electroreduction system, emphasizing the importance of the indirect reduction mechanism in the process. The H*/PDS system was further evaluated by degrading several model contaminants (10 μM). As shown in **Fig. 6a**, all these organics can be abated with removal efficiencies of more than 80% in 60 min. Fitting these degradation process with first-order kinetics unrevealed that the resultant kinetic constants **(Table S3)** were at least 5 times than that in previous researches about electrochemically activating PDS (**Table S4**) [7-9]. And different from traditionally transitional-metal-involved AOPs where high valent cationic (HVC, such as Fe(IV), Cr(V), Mn(III), Cu(III)) and radicals ($^{\bullet}OH$, $SO_4^{\bullet-}$) all got involved in oxidizing organics [38-42], the H*/PDS system theoretically avoided the generation of HVC. This can be confirmed by analyzing the degradation intermediate using methyl phenyl sulfoxide (PMSO) as model contaminant, due that PMSO was converted into methyl phenyl sulfone ($PMSO_2$) by HVC, while phenylsulfinic acid ($PhSO_2$) was produced from the radical oxidation (**Fig. S9**) [39]. The concentration of $PMSO_2$ was monitored in the PMSO

degradation process (**Fig. 6b**), the results revealed that nearly no signal of $PMSO_2$ appeared through the H*/PDS oxidation process. Excluding the HVC as ROS in the H*/PDS allowed engineers to controllably steer the decontamination process via a scheduled degradation route, while organics degradation (such as various sulfoxide contaminants) was possibly oriented to unexpected products by HVC in the PDS oxidation system [39, 43]. Additionally, different from the M^{n+}/PDS system, the H*-PDS system had less dependence on the solution pH (**Text S3**), because the atomic H* can be evolved from H^+ at acidic condition, while it came from the H_2O at alkaline/neutral solution [16]. Meanwhile, the acidification in the PDS-based oxidation process highly alleviated the possible effect of solution pH on the system.

The endurability of Pd/Al_2O_3 was monitored by recycling the catalyst in the H*/PDS system for 6 times. In these cycles, the performance on the BA degradation was kept at a high level (>80%) **(Fig. S10)**. Accordingly, nearly no dissolved Pd was detected by ICP-OES analysis, demonstrating no loss of active sites on the catalyst. Meanwhile, the XPS analysis (**Fig. S11a** and **S11b**, 335.8 eV for Pd^0 $3d_{5/2}$ and 341.1 eV for Pd^0 $3d_{3/2}$) revealed that the Pd on the used electrode was still kept at Pd^0 species, even after several cycles. The XRD results of the used electrode was also unraveled that the crystal face didn't change in the process (**Fig.S11c**). The excellent stability of Pd/Al_2O_3 catalyst, zero-addition property of transition metal catalyst, and pH-independent nature endowed the system with high potential for a ternary process of wastewater before the emission to the natural waters. However, taking the low efficiency of PDS activation into consideration, other materials with high performance on atomic H* generation and inhibition of direct electron transfer mechanism should be explored to reduce the PDS dosage and sulfate residue, and improve the application value of electro-activated PDS technology.

4. Conclusion

In this study, an electroreduction system for activating PDS and degrading organic contaminants was constructed using Pd/Al_2O_3 catalyst as particle electrode. The reactive oxygen species were determined to be $SO_4^{\bullet-}$/$^{\bullet}OH$ by ESR analysis, quenching experiments and PMSO degradation analysis. Furthermore, the single-electron reduction of PDS by electrogenerated atomic H* can readily form $SO_4^{\bullet-}$ (indirect reduction mechanism), through which the energy barrier (ΔG_{ds}) was determined to be only 0.92 eV by density functional theory analysis. By contrast, taking Pd-activated H_2 as electron donor, the PDS decomposition via direct electron transfer was unveiled difficult to yield $SO_4^{\bullet-}$ (ΔG_{ds}=4.28 eV), but smoothly steered towards inert SO_4^{2-} (ΔG_{ds}=0.54 eV). By optimizing the operation parameters to maximize the production of electro-induced atomic H*, the cathodic cell can efficiently activate PDS and degrade various organic pollutants with varying the kinetic constants from 0.0256 min^{-1} to 0.0645 min^{-1}, which were (5~15)-fold higher than that in previous studies. This research pointed out the importance of indirect reduction mechanism in the PDS activation process, which paved the way to rationally construct efficient materials for electrochemically activating PDS and subsequent decontamination of organic compounds by weakening the direct electron transfer and enhancing the atomic H*-mediated reduction mechanism.

Author information

Corresponding Author

Email: hclan@tsinghua.edu.cn. Tel: 86-10-62849160.

Notes

The authors declare no competing financial interest.

Supplementary Material

The Supplementary Material is available free of charge, including 4 Texts, 11 Figures, and 4 Tables.

Acknowledgements

The authors acknowledge financial support by National Natural Science Foundation of China (No. 51722811, 51978373).

References

[1] B.C. Hodges, E.L. Cates, J.H. Kim, Challenges and prospects of advanced oxidation water treatment processes using catalytic nanomaterials, Nat. Nanotechnol. 13 (2018) 642-650.

[2] J. Lee, U. von Gunten, J.-H. Kim, Persulfate-Based Advanced Oxidation: Critical Assessment of Opportunities and Roadblocks, Environ. Sci. Technol. 54 (2020) 3064-3081.

[3] P.D. Hu, M.C. Long, Cobalt-catalyzed sulfate radical-based advanced oxidation: A review on heterogeneous catalysts and applications, Appl. Catal. B-Environ. 181 (2016) 103-117.

[4] L.W. Matzek, K.E. Carter, Activated persulfate for organic chemical degradation: A review, Chemosphere 151 (2016) 178-188.

[5] G.P. Fan, L. Cang, G.D. Fang, D.M. Zhou, Surfactant and oxidant enhanced electrokinetic remediation of a PCBs polluted soil, Sep. Purif. Technol. 123 (2014) 106-113.

[6] F. Pardo, A. Santos, A. Romero, Fate of iron and polycyclic aromatic hydrocarbons during the remediation of a contaminated soil using iron-activated persulfate: A column study, Sci. Total Environ. 566 (2016) 480-488.

[7] L.W. Matzek, M.J. Tipton, A.T. Farmer, A.D. Steen, K.E. Carter, Understanding Electrochemically Activated Persulfate and Its Application to Ciprofloxacin Abatement, Environ. Sci. Technol. 52 (2018) 5875-5883.

[8] W.S. Chen, Y.C. Jhou, C.P. Huang, Mineralization of dinitrotoluenes in industrial wastewater by electro-activated persulfate oxidation, Chem. Eng. J. 252 (2014) 166-172.

[9] W.S. Chen, C.P. Huang, Mineralization of aniline in aqueous solution by electrochemical activation of persulfate, Chemosphere 125 (2015) 175-181.

[10] S.H. Yuan, P. Liao, A.N. Alshawabkeh, Electrolytic Manipulation of Persulfate Reactivity by Iron Electrodes for Trichloroethylene Degradation in Groundwater, Environ. Sci. Technol. 48 (2014) 656-663.

[11] A.I.A. Chowdhury, J.I. Gerhard, D. Reynolds, D.M. O'Carroll, Low Permeability Zone Remediation via Oxidant Delivered by Electrokinetics and Activated by Electrical Resistance Heating: Proof of Concept, Environ. Sci. Technol. 51 (2017) 13295-13303.

[12] H. Zeng, X. Zhao, F. Zhao, Y. Park, M. Sillanpää, Accelerated Fe^{3+}/Fe^{2+} Cycle using Atomic H* on Pd/Al_2O_3: A Novel Mechanism for an Electrochemical System with Particle Electrode for Iron Sludge Reduction in the Fe^{2+}/Peroxydisulfate Oxidation Process, Chem. Eng. J. (2019) 122972.

[13] R. Mao, N. Li, H.C. Lan, X. Zhao, H.J. Liu, J.H. Qu, M. Sun, Dechlorination of Trichloroacetic Acid Using a Noble Metal-Free Graphene-Cu Foam Electrode via Direct Cathodic Reduction and Atomic H*, Environ. Sci. Technol. 50 (2016) 3829-3837.

[14] J.-Y. Lee, J.G. Lee, S.-H. Lee, M. Seo, L. Piao, J.H. Bae, S.Y. Lim, Y.J. Park, T.D.J.N.c. Chung, Hydrogen-atom-mediated electrochemistry, Nat. Commun, 4 (2013) 2766.

[15] Y. Pan, H.R. Su, Y.T. Zhu, F.V. Molamahmood, M. Long, CaO_2 based Fenton-like reaction at neutral pH: Accelerated reduction of ferric species and production of superoxide radicals, Water Res. 145 (2018) 731-740.

[16] Y. Zheng, Y. Jiao, M. Jaroniec, S.Z. Qiao, Advancing the Electrochemistry of the Hydrogen-Evolution Reaction through Combining Experiment and Theory, Angew. Chem.-Int. Edit., 54 (2015) 52-65.

[17] A. Li, X. Zhao, Y. Hou, H. Liu, L. Wu, J. Qu, The electrocatalytic dechlorination of chloroacetic acids at electrodeposited Pd/Fe-modified carbon paper electrode, Appl. Catal. B-Environ. 111 (2012) 628-635.

[18] G.M. Jiang, M.N. Lan, Z.Y. Zhang, X.S. Lv, Z.M. Lou, X.H. Xu, F. Dong, S. Zhang, Identification of Active Hydrogen Species on Palladium Nanoparticles for an Enhanced Electrocatalytic Hydrodechlorination of 2,4-Dichlorophenol in Water, Environ. Sci. Technol. 51 (2017) 7599-7605.

[19] Y.J. Zhou, G. Zhang, Q.H. Ji, W. Zhang, J.Y. Zhang, H.J. Liu, J.H. Qu, Enhanced Stabilization and Effective Utilization of Atomic Hydrogen on Pd-In Nanoparticles in a Flow-through Electrode, Environ. Sci. Technol. 53 (2019) 11383-11390.

[20] X. Zhao, A. Li, R. Mao, H. Liu, J. Qu, Electrochemical removal of haloacetic acids in a three-dimensional electrochemical reactor with Pd-GAC particles as fixed filler and Pd-modified carbon paper as cathode, Water Res. 51 (2014) 134-143.

[21] P. Nate, V. Madhavan, H. Zemel, R. Fessenden, Rate constants and mechanism of reaction of $SO_4^{\cdot -}$ with aromatic compounds, J. Am. Chem. Soc. 99 (1977) 163-164.

[22] H.B. Zeng, S.S. Liu, B.Y. Chai, D. Cao, Y. Wang, X. Zhao, Enhanced Photoelectrocatalytic Decomplexation of Cu-EDTA and Cu Recovery by Persulfate Activated by UV and Cathodic Reduction, Environ. Sci. Technol. 50 (2016) 6459-6466.

[23] M.D. Segall, P.J.D. Lindan, M.J. Probert, C.J. Pickard, P.J. Hasnip, S.J. Clark, M.C. Payne, First-principles simulation: ideas, illustrations and the CASTEP code, J. Phys. Condens. Matter 14 (2002) 2717-2744.

[24] J.P. Perdew, K. Burke, M. Ernzerhof, Generalized gradient approximation made simple, Phys. Rev. Lett. 77 (1996) 3865-3868.

[25] D.R. Hamann, M. Schluter, C. Chiang, Norm-Conserving pseudopotentials, Phys. Rev. Lett. 43 (1979) 1494-1497.

[26] H.H. Li, Y. Wu, C. Li, Y.Y. Gong, L.Y. Niu, X.J. Liu, Q. Jiang, C.Q. Sun, S.Q. Xu, Design of Pt/t-ZrO_2/g-C_3N_4 efficient photocatalyst for the hydrogen evolution reaction, Appl. Catal. B-Environ., 251 (2019) 305-312.

[27] M.C. Militello, S. Simko, Elemental palladium by XPS, Surf. Sci. Spectra 3 (1994) 387-394.

[28] B.J. Tan, K.J. Klabunde, P.M.A. Sherwood, XPS studies of solvated metal atom dispersed (SMAD) catalysts. Evidence for layered cobalt-manganese particles on alumina and silica, J. Am. Chem. Soc. 113 (1991) 855-861.

[29] P. Quaino, E. Santos, Hydrogen Evolution Reaction on Palladium Multilayers Deposited on Au(111): A Theoretical Approach, Langmuir 31 (2015) 858-867.

[30] H.C. Lan, R. Mao, Y.T. Tong, Y.Z. Liu, H.J. Liu, X.Q. An, R.P. Liu, Enhanced Electroreductive Removal of Bromate by a Supported Pd-In Bimetallic Catalyst: Kinetics and Mechanism Investigation, Environ. Sci. Technol. 50 (2016) 11872-11878.

[31] C.J. Liang, H.W. Su, Identification of Sulfate and Hydroxyl Radicals in Thermally Activated Persulfate, Ind. Eng. Chem. Res. 48 (2009) 5558-5562.

[32] A. Rastogi, S.R. Ai-Abed, D.D. Dionysiou, Sulfate radical-based ferrous-peroxymonosulfate oxidative system for PCBs degradation in aqueous and sediment systems, Appl. Catal. B-Environ. 85 (2009) 171-179.

[33] V. Kavitha, K. Palanivelu, The role of ferrous ion in Fenton and photo-Fenton processes for the degradation of phenol, Chemosphere 55 (2004) 1235-1243.

[34] G.F. Wei, Y.H. Fang, Z.P. Liu, First Principles Tafel Kinetics for Resolving Key Parameters in Optimizing Oxygen Electrocatalytic Reduction Catalyst, J. Phys. Chem. C. 116 (2012) 12696-12705.

[35] Y. Feng, P.H. Lee, D.L. Wu, K.M. Shih, Surface-bound sulfate radical-dominated degradation of 1,4-dioxane by alumina-supported palladium (Pd/Al_2O_3) catalyzed peroxymonosulfate, Water Res. 120 (2017) 12-21.

[36] Y. Xu, H. Lin, Y.K. Li, H. Zhang, The mechanism and efficiency of MnO_2 activated persulfate process coupled with electrolysis, Sci. Total Environ., 609 (2017) 644-654.

[37] A. Georgi, M.V. Polo, K. Crincoli, K. Mackenzie, F.D. Kopinke, Accelerated Catalytic Fenton Reaction with Traces of Iron: An Fe-Pd-Multicatalysis Approach, Environ. Sci. Technol. 50 (2016) 5882-5891.

[38] H.Y. Dong, Y. Li, S.C. Wang, W.F. Liu, G.M. Zhou, Y.F. Xie, X.H. Guan, Both Fe(IV) and Radicals Are Active Oxidants in the Fe(II)/Peroxydisulfate Process, Environ. Sci. Technol. Lett. 7 (2020) 219-224.

[39] Z. Wang, J. Jiang, S.Y. Pang, Y. Zhou, C.T. Guan, Y. Gao, J. Li, Y. Yang, W. Qu, C.C. Jiang, Is Sulfate Radical Really Generated from Peroxydisulfate Activated by Iron(II) for Environmental Decontamination? Environ. Sci. Technol. 52 (2018) 11276-11284.

[40] H.Y. Dong, G.F. Wei, T.C. Cao, B.B. Shao, X.H. Guan, T.J. Strathmann, Insights into the Oxidation of Organic Cocontaminants during Cr(VI) Reduction by Sulfite: The Overlooked Significance of Cr(V), Environ. Sci. Technol. 54 (2020) 1157-1166.

[41] W.F. Liu, B. Sun, J.L. Qiao, X.H. Guan, Influence of Pyrophosphate on the Generation of Soluble Mn(III) from Reactions Involving Mn Oxides and Mn(VII), Environ. Sci. Technol. 53 (2019) 10227-10235.

[42] L.H. Wang, H.D. Xu, N. Jiang, Z.M. Wang, J. Jiang, T. Zhang, Trace Cupric Species Triggered Decomposition of Peroxymonosulfate and Degradation of Organic Pollutants: Cu(III) Being the Primary and Selective Intermediate Oxidant, Environ. Sci. Technol. 54 (2020) 4686-4694.

[43] C. Tai, J.F. Peng, J.F. Liu, G.B. Jiang, H. Zou, Determination of hydroxyl radicals in advanced oxidation processes with dimethyl sulfoxide trapping and liquid chromatography, Anal. Chim. Acta 527 (2004) 73-80.

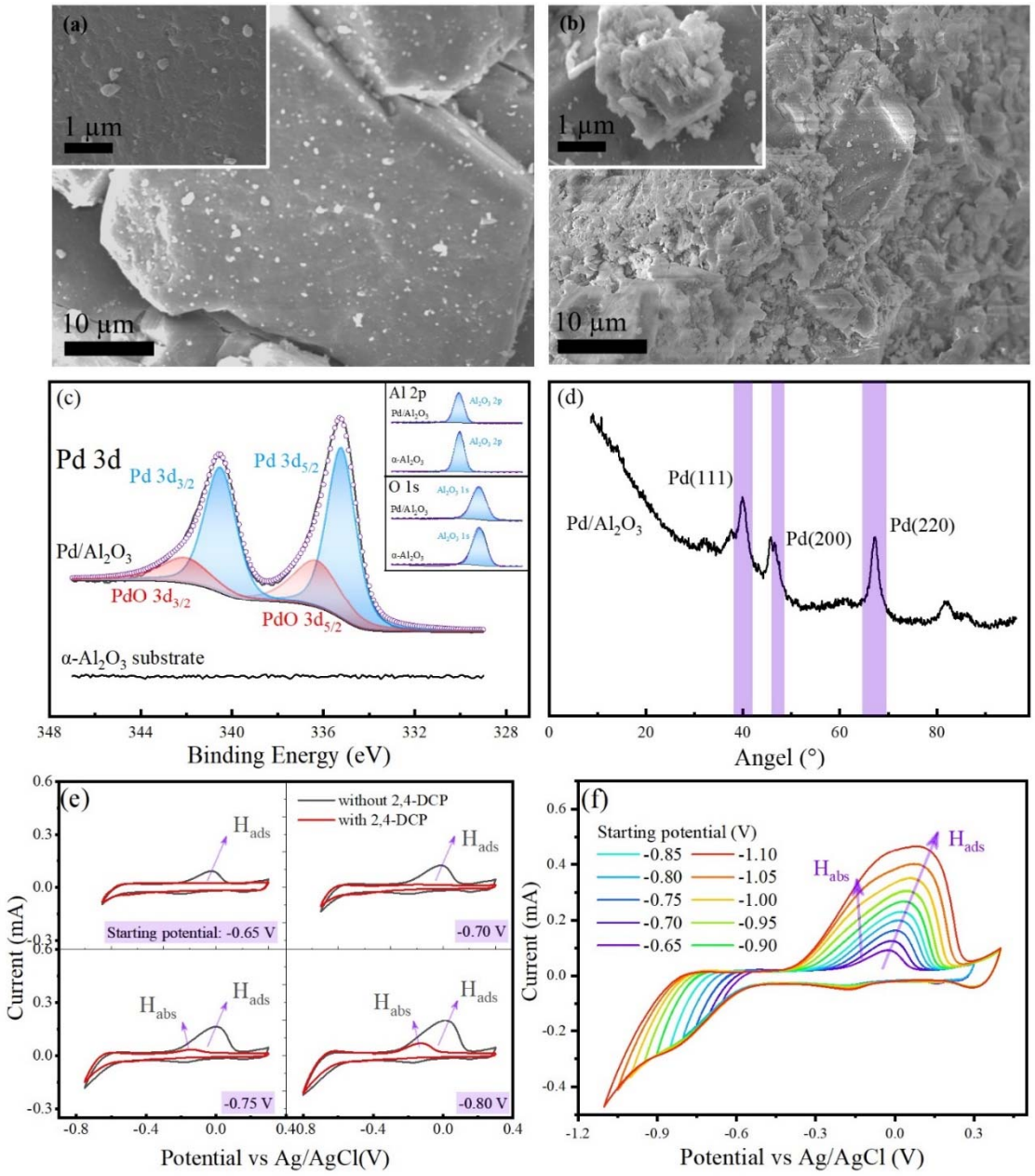

Fig. 1. SEM analyses of α-Al_2O_3 substrate (a) and Pd/Al_2O_3 catalyst (b); XPS analyses (c) and XRD analyses (d) of α-Al_2O_3 substrate and Pd/Al_2O_3 catalyst; (e) CVs of the Pd catalyst in N_2-saturated 50 mmol·L^{-1} Na_2SO_4 solution with and without 2,4-DCP under different starting potentials; (f) CVs of the Pd catalyst in N_2-saturated 50 mM Na_2SO_4 solution with different CV starting potentials: from −0.65 to −1.10 V. (scanning rate, 50 mV s^{-1}; solution pH, 7.0).

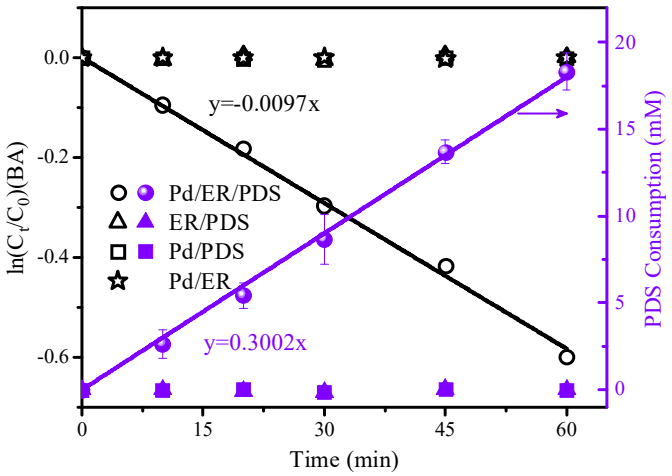

Fig. 2. BA degradation and PDS consumption in ER/PDS, Pd/PDS, Pd/ER and Pd/ER/PDS process. (BA, 50 μM; PDS, 20 mM; Pd/Al_2O_3, 0.5 g/L; Applied current, 0.10 A; initial solution pH, 3.0; deoxygenated atmosphere)

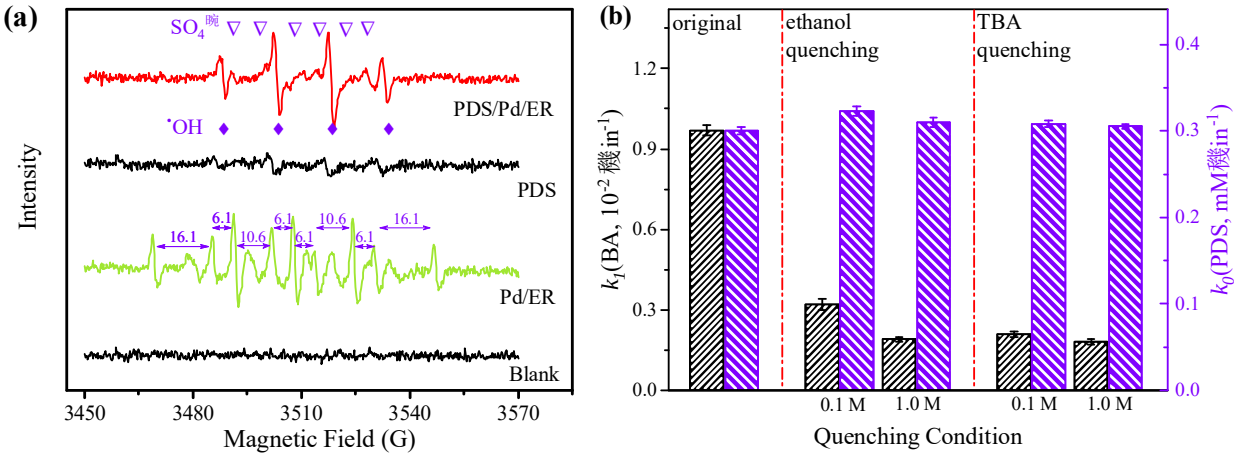

Fig. 3. (a) Identification of reactive species by ESR analysis; (b) *k*-value comparison of BA degradation (k_1) and PDS consumption (k_0) under different quenching conditions. (BA, 50 μM; PDS, 20 mM; Pd/Al_2O_3, 0.5 g/L; Applied current, 0.10 A; initial solution pH, 3.0; deoxygenated atmosphere)

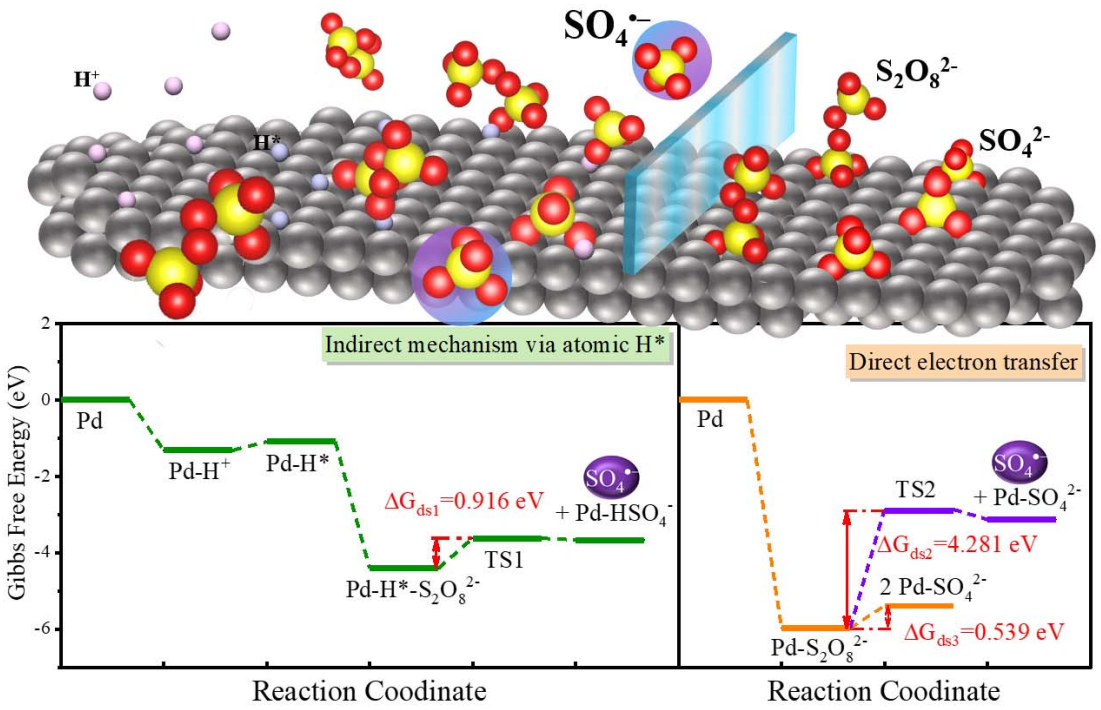

Fig. 4. Gibbs free energy variation for PDS decomposition on Pd(111) facet via different reduction approaches: indirect reduction via atomic H* and direct electron transfer.

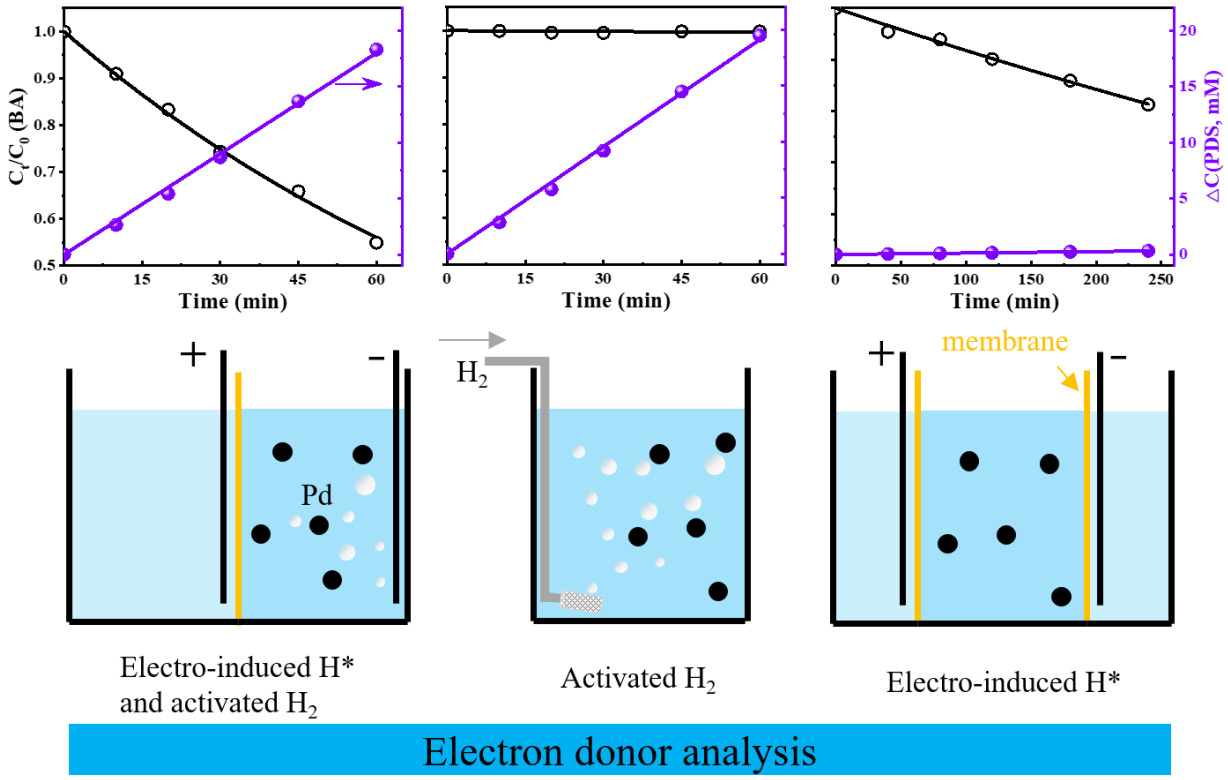

Fig. 5. The effect of different approaches for atomic H* generation on the BA degradation and PDS decomposition. (BA, 50 μM; PDS, 20 mM; Pd/Al_2O_3, 0.5 g/L; applied current, 0.10 A; initial solution pH, 3.0; deoxygenated atmosphere)

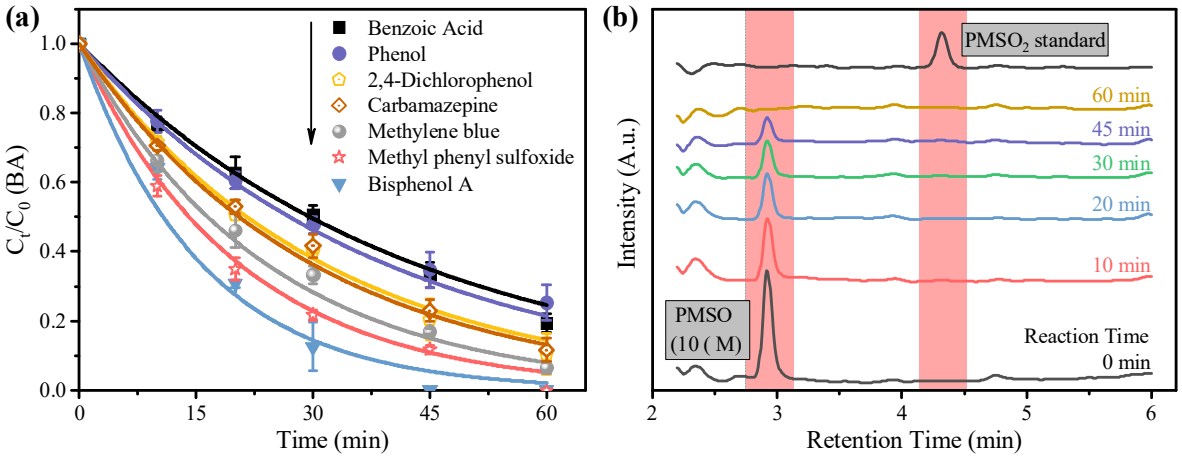

Fig. 6. (a) Degradation performance on various organics in the H*/PDS system; (b) the HPLC spectra of samples in the H*/PDS system. ([Organic compounds], 10 μM; [Pd/Al_2O_3], 0.5 g/L; [PDS], 20 mM; current, 0.1 A; solution pH 3.0; λ_{HPLC}, 230 nm)

Table. 1. Effect of the applied current, PDS concentration and Pd/Al_2O_3 dosage on the kinetics constants (*k*-value) of PDS consumption and BA degradation. (BA, 50 μM; initial solution pH, 3.0; deoxygenated atmosphere)

No.	Current (A)	C(PDS) (mM)	C(Pd/Al_2O_3) (g/L)	k_1 (BA) (min^{-1})	k_0 (PDS) (mM/min)
1.	0.1	20	0.5	0.0097	0.2982
2.	0.05	20	0.5	0.0051	0.1595
3.	0.02	20	0.5	0	0.0657
4.	0.1	20	1.0	0.0169	0.3026
5.	0.1	20	0.2	0.0031	0.3163
6.	0.1	20	0.1	0.0019	0.3121
7.	0.1	50	0.5	0.0087	0.3002
8.	0.1	10	0.5	0.0074	0.2802